

Light particle emission in the reaction $^{144}\text{Sm}(^{32}\text{S}, \text{fission})$ at $E_{\text{lab}} = 838 \text{ MeV}$

F. Benrachi, B. Chambon, B. Cheynis, D. Drain, and C. Pastor

Institut de Physique Nucléaire de Lyon, Institut National de Physique Nucléaire et de Physique des Particules, Centre National de la Recherche Scientifique, Université Claude Bernard, 43 Boulevard du 11 Novembre 1918, F-69622 Villeurbanne Cedex, France

H. Rossner, D. Hilscher, B. Gebauer, and D. Husson

Hahn-Meitner-Institut Berlin, D-14091 Berlin, Germany

A. Giorni, D. Heuer, A. Lleres, P. Stassi, and J. B. Viano

Institut des Sciences Nucléaires de Grenoble, Institut National de Physique Nucléaire et de Physique des Particules, Centre National de la Recherche Scientifique, Université Joseph Fourier, 53 Avenue des Martyrs, F-38026 Grenoble Cedex, France

(Received 6 July 1993)

Energy spectra of light charged particles have been measured in coincidence with fissionlike fragments using the 4π charged-particle detector AMPHORA. Preequilibrium, pre-scission, and post-scission components of emitted protons, deuterons, and alphas have been extracted from the energy spectra using a multiple source fit procedure. Including previously measured exclusive neutrons, a complete data set for light particle emission from the system $^{144}\text{Sm} + ^{32}\text{S}$ (26 A MeV) is now available. Mass and excitation energy of an equilibrated composite system has been defined by application of the massive transfer model using multiplicities and apparent temperatures of the pre-equilibrium components. The results have been compared to statistical model computations. A fair overall agreement is observed for different parametrizations of the Fermi-gas level-density parameter with indications for a decrease of the level density parameter with increasing nuclear temperature. The correlations between slope parameter, pre-scission, and total particle multiplicity turned out to be a sensitive probe for the level density parameter. In the energy spectra of alpha particles a low-energy component has been observed with strong focusing into directions perpendicular to the fission axis.

PACS number(s): 25.70.Jj, 24.60.Dr

I. INTRODUCTION

The investigation of macroscopic properties of hot nuclear matter, like temperature, moment of inertia, size, shape, and viscosity, is an object of vivid current interest in nuclear physics and is usually performed by experiments using heavy-ion reactions at bombarding energies between 10 and 100 MeV per nucleon [1–3]. Information about the nucleus is deduced from measurements of gamma rays, light particles, and fragments, and numerical values about the macroscopic properties of highly excited nuclei were frequently extracted by application of the statistical model. This model assumes an equilibrated composite system whose decay is governed by the available phase space. Especially it can be shown that in first approximation the square of the nuclear temperature is proportional to the thermal excitation energy: $E^* = aT^2$, where the factor a is the level density parameter of the excited nucleus. This parameter in conjunction with the inverse reaction cross section (or transmission coefficient) also describes yield and shape of the energy spectra of emitted particles.

At excitation energies above 100 MeV the application of the statistical model is getting questionable, because of uncertainties in the level density and because of doubts on the Fermi-gas model, which is mostly used to get the familiar and convenient form of the level density. As

pointed out earlier [4,5] a serious drawback of the Fermi-gas level density is the assumption of an infinitely deep potential well for the independently moving particles. If this well is replaced by a more realistic one with finite depth, then states which were originally situated within the well might now turn into resonance states in the continuum, with lifetimes considerably shorter than the equilibration time of the compound nucleus. Those states should not be listed as compound nucleus states, and thus, with increasing excitation energy, a realistic level density should drop more and more below a Fermi-gas level density. An indication of this effect is the observation of the decrease of the Fermi-gas level-density parameter with increasing excitation energy [6,7].

Another feature of the statistical model is the placement of a “nuclear clock” at our disposal. The rate of neutron evaporation is used to define a “neutron clock” and, including the competition between fission and particle evaporation, a time scale for fission can be constructed. The time scale strongly depends on the level density used, and a more stringent test of this method would be to include the corresponding “charged particle clock” as well.

The motivation for the experiment described here was to test the statistical model at high excitation energies ($\approx 500 \text{ MeV}$) by comparison of particle multiplicities and slope parameters of the energy spectra of pre- and

postsission evaporated particles, and by comparison of the “neutron clock” and the “charged particle clock”. The system $^{144}\text{Sm} + ^{32}\text{S}$ (838 MeV) has been chosen to complete the neutron data measured previously in coincidence with fission fragments [8] by exclusive measurements of light charged particles (p, d, α). A preference for charged particle emission is expected for the composite system $^{144}\text{Sm} + ^{32}\text{S}$ relative to the neutron-rich system $^{154}\text{Sm} + ^{32}\text{S}$.

The dominant mechanisms of light particle emission are established, and the particle multiplicities associated with each mechanism are extracted. The total excitation energies E_{CN}^* and masses of the equilibrated composite systems formed after preequilibrium particle emission are determined from linear momentum transfer (LMT) measured with the folding angle technique. The experimental conditions were selected to get the maximum possible excitation energy compatible with a dominance of symmetric fission and to enhance selectivity for the binary component with an appropriate (i.e., planar) detector geometry. In addition, the excitation energies $E_{\text{CN}}^*(\text{LMT})$ extracted from the measured multiplicities of preequilibrium particles using the massive transfer model must be confronted with multiplicities and respective nuclear temperatures observed for the prescission particle source to yield a consistent level-density parameter for the statistical-model analysis.

The paper is organized as follows. In Sec. II the experimental procedure is described, which is followed by the presentation of the fragment and light charged particle spectra in Sec. III, where the moving source fit procedure and the azimuthal distribution of the composite system component is discussed. The statistical-model analysis is presented in Sec. IV, and a summary is given in Sec. V.

II. EXPERIMENTAL PROCEDURE

The experiment was accomplished at the System Accélérateur Rhône Alpes (SARA) coupled cyclotron facility in Grenoble, using ^{32}S projectiles of 838 MeV on ^{144}Sm of $315 \mu\text{g}/\text{cm}^2$. Light charged particles (p, d, α) were detected by AMPHORA CsI(Tl) detectors [9,10]. Kinematic coincidences between reaction products were detected by two position-sensitive low-pressure multiwire proportional chambers (MWPC). Each one had an area of $61 \times 61 \text{ mm}^2$. They replaced the standard CsI(Tl) detector units of ring 5 ($\langle \Theta \rangle = 46.7^\circ$) of AMPHORA. The mean detector angle of $\langle \Theta \rangle = 46.7^\circ$ had been chosen to select the most central collisions in this reaction [8]. The MWPC's were mounted at a distance of 340 mm from the target position and had an angular acceptance of $\pm 5^\circ$ in the x and y directions. They measured the in-plane and out-of-plane position of two heavy reaction products in addition to their relative and absolute flight times relative to SARA's radio frequency. The absolute time scale had been adjusted to previous measurements, and times and positions were used to determine the fragment velocity vectors in the laboratory system.

For the CsI(Tl) detectors the pulse shape discrimination method was used to identify light particles. This method allowed to separate protons, deuterons, and tri-

tons down to threshold energies of about 1.5 MeV per nucleon, whereas ^3He and alphas could not be separated at the lowest energies. Extrapolating the yield of ^3He into the low-energy regime we estimated the ratio $^3\text{He}/^4\text{He}$ to $\approx 3\%$. The energy calibration of the CsI(Tl) was accomplished by use of alpha sources (^{241}Am , ^{244}Cm , Th) and two alpha beams of 19 and 50 MeV bombarding gold and formvar targets. Linear relations between the energy deposited in the crystal and the light output (fast component) of the detector were obtained for protons and alphas in the forward hemisphere. The alpha-source data and these relations were used for the detectors in the backward hemisphere and using interpolation procedures for the energy calibration of the deuterons [11,12]. The energy calibration has been performed for each detector and each particle separately with an overall estimated uncertainty of 10%.

III. FRAGMENT AND LIGHT CHARGED PARTICLE SPECTRA

A. Linear momentum transfer

The velocity v_{CS} of the fissioning composite system is related by kinematics to the velocity components $v_{1,2\parallel}$ and $v_{1,2\perp}$ of the two fissionlike fragments parallel and perpendicular to the beam direction:

$$v_{\text{CS}} = \frac{v_{1\parallel}v_{2\perp} + v_{1\perp}v_{2\parallel}}{v_{1\perp} + v_{2\perp}}. \quad (1)$$

In Fig. 1 the Galilean invariant form of the velocity distribution for v_{CS} is shown and the velocity which corresponds to full momentum transfer is indicated by an arrow. Due to the time resolution of 1.8 ns in the flight time of the fragments, the systematic error of the absolute time scale, and the dispersion of the fragment velocity vectors due to pre- and postsission particle emission the uncertainty in v_{CS} is estimated to 12%.

Conservation of linear momentum leads to the relation between v_{CS} and the transferred fraction ρ of linear momentum:

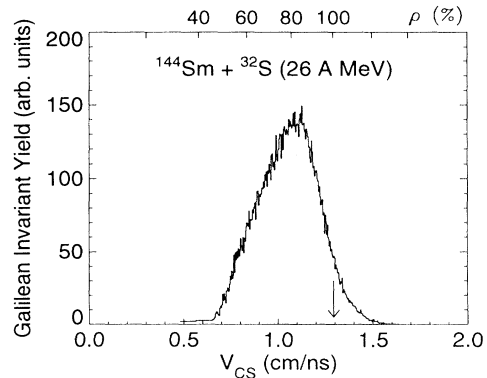


FIG. 1. Galilean invariant velocity distribution of the composite system as deduced from the fragment velocity vectors. The velocity of full momentum transfer is indicated by an arrow.

$$\rho = \frac{P_{\parallel}}{P_{\text{beam}}} = \frac{A_T}{A_T + A_P(1 - v_{\text{CS}}/v_{\text{CF}})} \frac{v_{\text{CS}}}{v_{\text{CF}}}. \quad (2)$$

The upper scale in Fig. 1 represents ρ using the velocity $v_{\text{CF}} = 1.293$ cm/ns for complete fusion, and $A_P = 32$ and $A_T = 144$, for projectile and target mass numbers. The mean momentum transfer deduced from the fragment velocity vectors is observed at 77% of the transfer for complete fusion.

B. Moving source parametrization

To extract macroscopic parameters of the emitting sources such as the apparent temperature T , multiplicity, and Coulomb barrier B_C of emitted particles, the experimental energy spectra measured in coincidence with the two fission fragments have been reproduced by a moving source fit. The energy distribution of emitted light particles in the source rest frame is written as

$$\frac{d^2\sigma}{d\Omega dE} \approx (E_{\text{c.m.}} - B')^{nb} \exp\left[\frac{-(E_{\text{c.m.}} - B_C)}{T}\right] W(\Phi) \quad (3)$$

with $n = 1$ for surface emission, $n = \frac{1}{2}$ for volume emission, and the azimuthal angular distribution is described by $W(\Phi)$. For above barrier energies we set $B' = B_C$ and $b = 1$; for sub-barrier energies we used $B' = (1 - b)T + B_C$ [13] with b adjusted at $E_{\text{c.m.}} = B_C$ to achieve smooth extrapolation into the sub-barrier energy regime ($1 \leq b \leq 4$).

The measured energy spectra were fitted assuming five sources: (1) the composite system with average velocity $\langle v_{\text{CS}} \rangle$, (2), and (3) the two fragments ($\Theta_1 = \Theta_2$) with average velocities $\langle v_1 \rangle = \langle v_2 \rangle$, (4) and intermediate source moving with half the beam velocity $\langle v_{\text{IS}} \rangle = v_{\text{beam}}/2$, and (5) a source with beam velocity v_{beam} . Nonisotropic particle emission has been assumed for source (1) [$W(180^\circ)/W(90^\circ) = 1.4, 1.1, \text{ and } 1.0$ for $\alpha, d, \text{ and } p$, respectively] (see Sec. III C), and isotropic emission for the sources (2)–(5).

The sources (4) and (5) were used as simple parametrization of the complicated process of preequilibrium emission and projectile breakup. In a naive picture like the massive transfer model, alphas from projectile break-up are expected at very forward angles only. However, com-

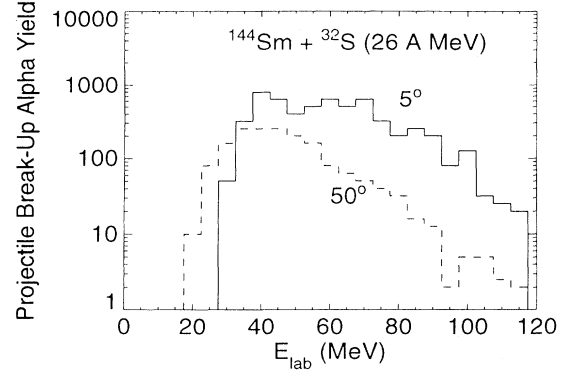


FIG. 2. Alpha energy spectra calculated by a classical model for dissipative projectile breakup at laboratory angles of 5° and 50° . Events are shown where not more than two alphas survive the capture process of the reaction $^{144}\text{Sm} + ^{32}\text{S}$.

putations with the more advanced model of Möhring, Srokowski, and Gross [14] indicate that, due to the slowing down and bending of projectile trajectories caused by frictional forces at the target surface, breakup alphas may also be expected with appreciable yield at larger angles, like $\theta_{\text{lab}} = 50^\circ$ (Fig. 2). This effect will cause a mixing of the contributions of particles emitted during projectile breakup and an intermediate source, and the parameters extracted for the two preequilibrium components have to be considered with caution. Using these multiplicities and velocities to estimate the linear momentum carried away by these preequilibrium particles, we infer a linear momentum transfer ratio of $\rho = 71\%$. Considering the rough approximation and the experimental uncertainties, this value is in agreement with the value of $\rho = 77\%$ deduced from the composite system velocity.

Maxwellian surface emission has been used for the fragment sources (2) and (3) with multiplicities below one, and volume emission has been assumed for the other sources [(1), (4), and (5)]. The barriers, multiplicities, and temperatures of the sources were searched for by a least-squares procedure assuming equal temperatures for the two fissionlike fragments. The deduced fit parameters are listed in Table I, and the total fit as well as the contributions of preequilibrium component [sources (4) and (5)], the composite system component [source (1)], and the

TABLE I. Results of the multiple source fit.

	Precision	Postscission	Interm. system	Projectilelike
M_p	5.4 ± 0.5	0.6 ± 0.2	1.7 ± 0.7	1.2 ± 0.5
T_p	5.5 ± 0.8	2.6 ± 1.1	11.0 ± 3.0	5.0 ± 2.1
B_p	10.9 ± 0.6	6.1 ± 1.1	13.2 ± 3.1	1.0 ± 0.8
M_d	1.1 ± 0.2	0.14 ± 0.07	0.9 ± 0.2	0.4 ± 0.2
T_d	5.8 ± 1.2	2.6 ± 1.5	14.5 ± 4.0	4.8 ± 3.0
B_d	15.1 ± 1.2	8.8 ± 5.4	13.4 ± 3.7	1.0 ± 1.1
M_α	3.2 ± 0.4	0.3 ± 0.2	1.1 ± 0.4	1.1 ± 0.4
T_α	6.6 ± 0.7	2.2 ± 0.8	12.7 ± 3.0	13.8 ± 1.5
B_α	19.9 ± 1.2	10.6 ± 4.0	4.6 ± 3.0	4.9 ± 2.7

fragment component [sources (2) and (3)] are shown in Figs. 3(a)–3(c) for p , d , and α .

C. Anisotropies

For fission reactions induced by low-energy heavy-ion reactions, the azimuthal correlation of the two fragments is strongly peaked at $\Delta\phi=180^\circ$. The width of the distribution is due to smearing of the angular correlation by pre- and postscission particle emission and by the finite granularity of the fragment detector. The dispersion will increase with increasing excitation energy and thus will cause more and more loss of resolution in the determination of the reaction plane which is defined by the velocity vectors of the two fragments. According to the modified

evaporation code JULIAN [15] the recoil effects of pre- and postscission particle evaporation cause an out-of-plane dispersion of 30° at full width at half maximum. These effects and uncertainties in shape and temperature of the emitting system prevent to extract reliable values for the spin of the composite system. When the azimuthal distribution $W(\Phi)$ is expressed as

$$W(\Phi) \propto \exp[-\beta \sin^2(\Phi)], \quad (4)$$

where Φ is the angle of the particle emission direction with respect to the reaction plane; the anisotropy parameter β can be expressed by macroscopic quantities of the emitting system:

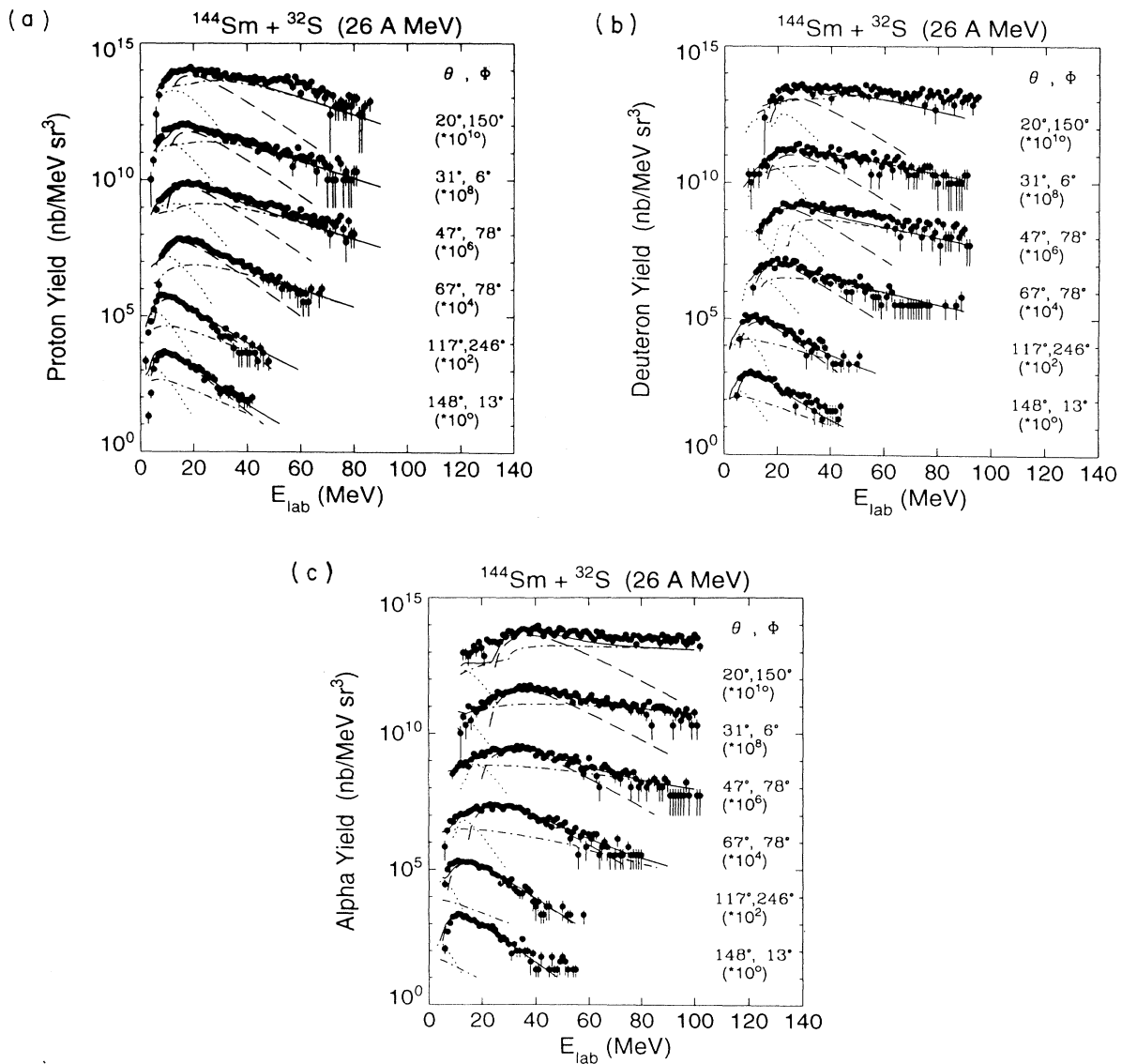


FIG. 3. (a) Proton energy spectra measured with AMPHORA detectors at the specified angles. The results of the five source fit are indicated by solid lines, dashed lines, dotted lines, and dash-dotted lines for the total fit, the composite system component, the sum of the fragment components, and the sum of the pre-equilibrium components, respectively. (b) Same as (a), but for deuterons. (c) Same as (a), but for alphas.

$$\beta = \frac{\hbar^2(J_i + \frac{1}{2})^2}{2TT} \frac{\mu R^2}{T + \mu R^2} \quad (5)$$

For instance, using a spin value of $J_i = 80$, a nuclear temperature of $T = 6.6$ MeV (see Table I), a moment of inertia T of a sphere containing 161 nucleons, and a reduced mass μ for alpha emission at a barrier radius $R = 10.6$ fm, we expect an anisotropy parameter of $\beta = 0.94$.

In addition to the uncertainties mentioned above, the azimuthal distribution can be disturbed by contributions of other sources, which are difficult to separate in a normal multiple source fit. This is demonstrated in Fig. 4(a), where energy spectra of alphas are shown for some in-plane and out-of-plane detectors. An additional low-energy component is observed in the α spectra of the

out-of-plane detectors ($\Phi = 264^\circ$). Such a component is essentially absent in the proton spectra [Fig. 4(b)]. To demonstrate the strong focusing of these additional low-energy particles into directions perpendicular to the fission fragment separation axis, we display in Fig. 5 the azimuthal distribution of both components normalized to the respective mean value. The low-energy component has been defined by an energy gate in the near-barrier region [left bar in Fig. 4(a)], where in-plane and out-of-plane spectra differ the most. The spectrum area within an energy gate close to the low-energy component [right bar in Fig. 4(a)] is hereafter referred to as regular component. As expected, this component, which represents alpha evaporation from rotating nuclei with spins perpendicular to the reaction plane, is peaked at ($\Phi \approx 0^\circ, 180^\circ, 360^\circ$), whereas the low-energy component displays maxima at angles perpendicular to this plane ($\Phi \approx 90^\circ, 270^\circ$). For comparison, the normalized anisotropy function $W(\Phi)/\langle W \rangle$ has been calculated for different angles θ_{lab} using $\beta = 0.94$ and has been included in the figure (solid line). We conclude from kinematics that these particles are emitted from a source which moves with the composite system velocity. Such a behavior is consistent with emission of alphas from the neck region of a fissioning nucleus, as observed in low-energy [16] and in intermediate-energy fission [17].

It is noted that the two gates shown in Fig. 4(a) do not perform a clear separation between the different sources of the composite system, and, further, these components have not been treated separately in the multiple source fit procedure. Thus, the mixture of these components will result in lower average values and larger variances for Coulomb barriers and anisotropies of the composite system.

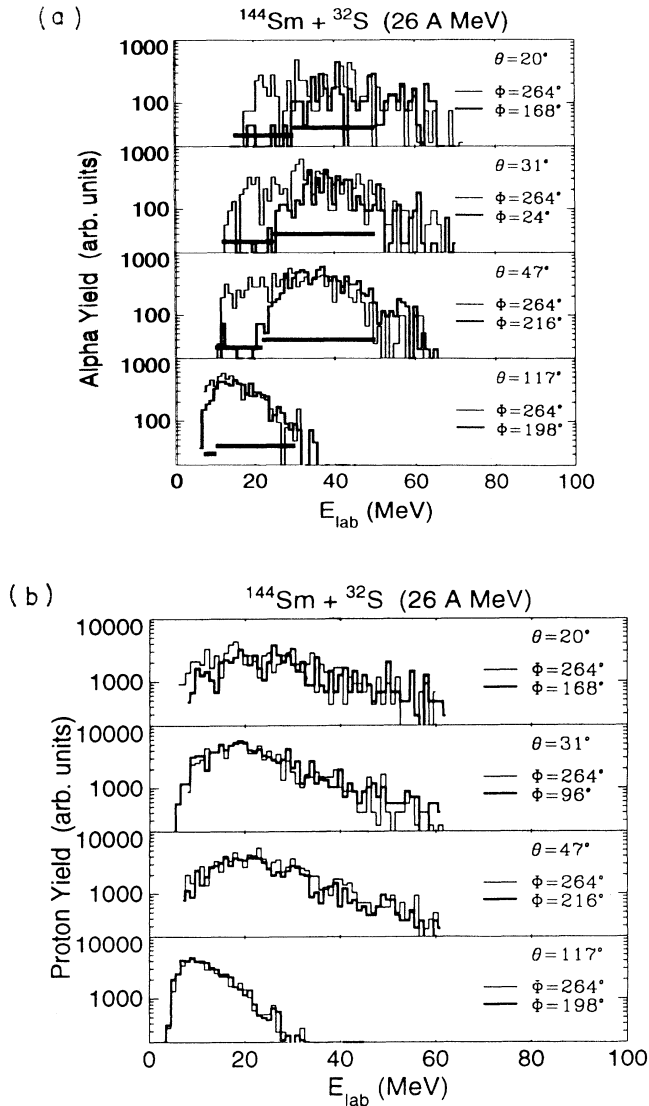


FIG. 4. (a) Alpha energy spectra for some in-plane and out-of-plane detector positions. The bars indicate the energy regions used for the plot of Fig. 5. (b) Proton energy spectra for some in-plane and out-of-plane detector positions of (a).

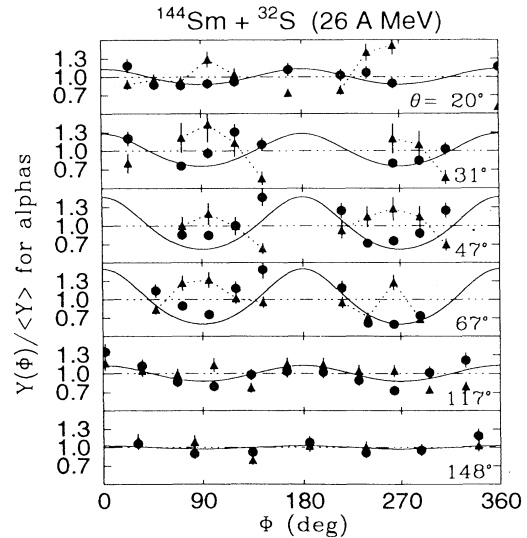


FIG. 5. Normalized azimuthal distribution of alphas. The filled triangles represent the yield in the low-energy region [left bars in Fig. 4(a)], the dots represent the yield in the energy region of the regular composite system component [right bars in Fig. 4(a)].

IV. STATISTICAL-MODEL ANALYSIS

A. Level-density parameters and transmission coefficients

The reaction is assumed to occur in three steps: formation of a composite system, pre-equilibrium particle emission during the equilibration process, and decay of the compound nucleus. We further assume that the formation time is short compared to the evaporation time and that particle evaporation is negligible during that time. It is, of course, not possible to draw a sharp line between pre-equilibrium and equilibrium particle emission and we have to rely on the multiple source fit procedure to separate compound and noncompound components in the particle energy spectra. The statistical model addresses the decay probability after the equilibration process is completed. Within this model the particle evaporation process is governed by two basic quantities, the spin-dependent level-density parameter and the transmission coefficients. Therefore the shape of the energy spectra carries information about the level density (or temperature) and the size and deformation of the compound nucleus.

A phenomenological ansatz is used for the level density taking into account the influence of surface area and shape of the nucleus [18]. The deformation dependence of the level-density parameter a is expressed as

$$a(A) = a_V A + a_S A^{2/3} B_S + a_K A^{1/3} B_K, \quad (6)$$

where the coefficients a_V , a_S , and a_K describe the volume, the surface, and the curvature terms, respectively. B_S and B_K are the values of the surface area and average curvature of a nucleus relative to a sphere of equal size. So, for the liquid drop ground state, these quantities are one ($B_S = B_K = 1$), and for the saddle configuration they are functions of the fissility [19]. Values for the coefficients a_V , a_S , and a_K were published by several authors. We have used the three sets listed in Table II.

The largest dependence of the level density on nuclear deformation results for the set of Töke and Swiatecki (TS) and the smallest dependence is given by the set of Ignatyuk. In the last column the average value of the level density parameter is given for the composite system studied in this work (Sec. IV B and Table III).

The transmission coefficients which control access to the available phase space are usually generated from published optical-model parameters for spherical nuclei. Energy spectra of evaporated charged particles calculated with these transmission coefficients often show barrier heights in excess of the experimentally observed emission barriers. Also, these parametrizations, being based on elastic-scattering data, exhibit features (especially for

TABLE II. Level-density parameters.

Author	a_V	a_S	a_K	$\langle a \rangle$
Ignatyuk [26]	0.073	0.095	0.000	11.06
Reisdorf [27]	0.069	0.179	0.164	9.31
TS [28]	0.0685	0.213	0.384	8.30

TABLE III. Excitation energies for different momentum transfers.

	$\rho(\%)$	Q (MeV)	E^* (MeV)	Initial nuclei
0α	86.24	-77.56	529	8000
-1α	73.74	-64.96	466	8000
-2α	61.24	-49.89	402	4000

neutrons and protons) like volume transparency, shape resonances, and surface absorption, which are not related to the evaporation process [20].

In our calculations we applied transmission coefficients computed as

$$T_l = \{1 + \exp[(B_l - E)2\pi/\hbar\omega]\}^{-1}, \quad (7)$$

with

$$B_l = Z_1 Z_2 e^2 / r_C + l(l+1)\hbar^2 / (2\mu r_l^2).$$

The Coulomb radius r_C and the radius r_l of the moment of inertia are parameterized as

$$r_{C,I} = r_{0,C,I} (A_1^{1/3} + A_2^{1/3}) + d.$$

The parameters $r_{0,C}$, $r_{0,I}$, d , and $\hbar\omega$ have been adjusted to fit the optical-model reaction cross sections of neutrons [21], protons [22], deuterons [23], and alphas [24]. In Fig. 6 the deduced barriers $B_{l=0}$ for protons and alphas (crosses connected by lines) are compared with the empirical fusion barriers (small dots and diamonds) as given in Ref. [25]. The barriers extracted from the optical-model reaction cross section are, in fact, slightly higher than the fusion barriers. We also included in Fig. 6 the barriers for protons and alphas (large plot symbols), extracted from our multiple source fit. These barriers are consistent with the empirical fusion barriers.

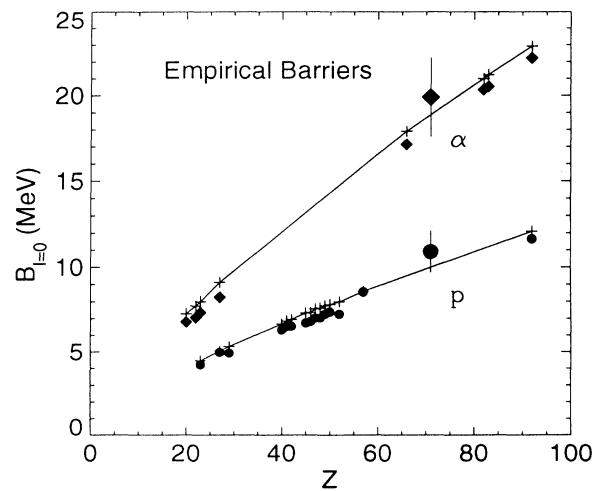


FIG. 6. Comparison of the emission barriers for protons (diamonds) and alphas (dot) as deduced from the multiple source fit (large symbols) with empirical fusion barriers (small symbols) and barriers deduced from optical model parameters (crosses connected by lines).

B. Excitation energy and spin distribution

The massive transfer model combined with particle emission from an intermediate source and from a compound nucleus has been used to interpret the velocity distribution of the composite system (Sec. III A). It is assumed that the finite time resolution, recoil effects due to particle emission, and different entrance channels due to projectile breakup, are resulting in the measured width of the distribution. According to JULIAN calculations the recoil effects of particle evaporation from the composite system cause a spread in the intermediate source velocity of $\Delta v_{CS} \approx \pm 0.15$ cm/ns, and thus prevent considering projectile breakup in smaller partitions but alpha particles.

An initial momentum transfer ratio ρ_j was defined assuming that the momentum P_j was carried away in beam direction by j alpha particles ($j=0,1,2$) in addition to the momentum P_{IS} of the intermediate source particles:

$$\rho_j = [P_p - P_{IS} - P_j] / P_p, \quad (8)$$

$$P_{IS} = \sum_i (M_i A_i) m_0 v_i.$$

P_p is the momentum of the projectile and M_i , A_i , m_0 , and v_i represent the particle multiplicity, the mass number, the nucleon mass, and the velocity of the intermediate source, respectively. The sum includes n , p , d , and α 's, and the corresponding values for charged particles were taken from Table I and those for neutrons were taken from an earlier experiment [8] ($M_n = 2.7$, $T_n = 12.0$ MeV).

The excitation energy of the equilibrated composite system after complete ($j=0$) and incomplete fusion ($j=1,2$) is then written as

$$E_{CN,j}^* = E_p A_T / (A_p + A_T / \rho_j) + Q(\rho_j), \quad (9)$$

where E_p , A_p , A_T , and $Q(\rho_j)$ represent the incident energy, the mass number of projectile and target, and the Q value of the specific reaction. In the evaporation calculations the numbers of initial compound nuclei N_j with excitation energy $E_{CN,j}^*$ were assumed in proportion to the yield of the velocity related to ρ_j . The results for ρ_j , $Q(\rho_j)$, E^* , and N_j are listed in Table III.

The spin distributions used in the statistical-model computations for the systems formed by complete and incomplete fusion are shown in Fig. 7. These distributions represent the results of a classical model for dissipative projectile breakup [14]. Modifications of the distributions due to pre-equilibrium particle emission were neglected, assuming the moderate changes of spin will not alter the partition between thermal and collective excitation energy significantly.

C. Comparison with experiment

The average lifetime τ of a compound nucleus at excitation energy E^* and spin I is given by the total decay width Γ :

$$\hbar / \tau(E^*, I) = \Gamma(E^*, I). \quad (10)$$

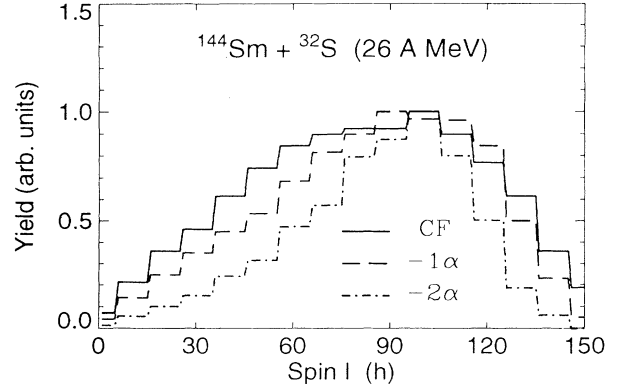


FIG. 7. Spin distributions for complete (CF) and incomplete capture (-1α , -2α) computed by a classical model of dissipative alpha breakup. The maximum of each individual yield has been normalized to 1.

This time is computed for each decay step in the nuclear cascade. The cumulative multiplicities of neutrons, protons, deuterons, and alpha particles for a progressive decay time are shown in Fig. 8. This dependence is the result of a statistical-model computation for a nonfissioning nucleus using the “Reisdorf” parametrization for the level-density parameter a . The experimental multiplicities including the errors are represented by dashed areas. From this figure we conclude that the measured pre-scission particle multiplicities can be explained by the statistical model if we assume an average lifetime of $\tau \approx 10^{-20}$ s of the composite system before scission. We further observe that τ is less sensitive to the pre-scission particle multiplicity for times $\tau > 10^{-20}$ s when most of the particles have already been evaporated.

The decline of the average excitation energy is shown in Fig. 9 using different parametrizations of the level density parameter. When fission occurs after $\approx 10^{-20}$ s, the

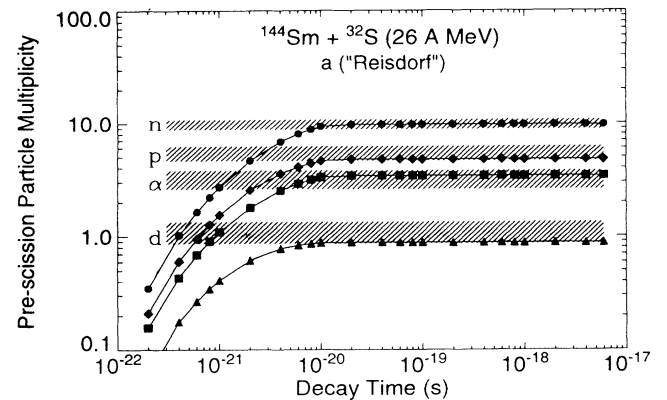


FIG. 8. Cumulative yield of neutrons, protons, deuterons, and alphas, computed by an evaporation code for the decay times of different decay steps. The “Reisdorf” parametrization of the level-density parameter has been used. The dashed areas represent the mean multiplicities and errors extracted from the multiple source fit.

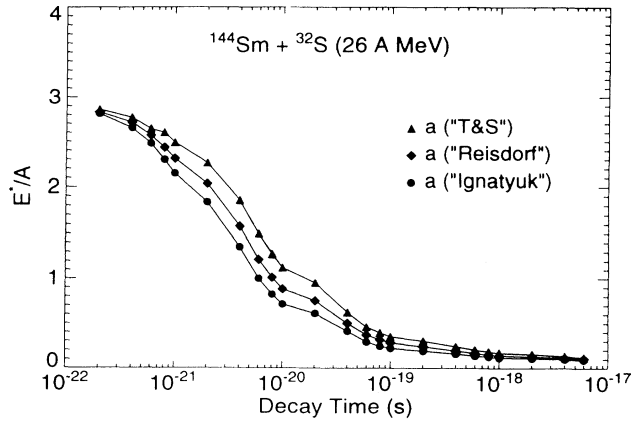


FIG. 9. Time evolution of the total excitation energy shown for different parametrizations of the level-density parameter.

remaining excitation energy given to the fragments will be different for different level densities. This effect is demonstrated in Fig. 10, where the correlation between pre-scission and total particle multiplicity is plotted. The results of the multiple source fit are represented by dashed areas which indicate the attributed errors, and the filled symbols describe the computations using a delay time for fission of $\tau_{\text{delay}} = 12 \times 10^{-21}$ s. With well-defined multiplicities this method can be used to get information about the level density of hot nuclei. Despite large experimental errors we observe, that the multiplicities of neutrons are better described by the TS parametrization, whereas charged particles, being emitted at higher excitation energies, favor the parametrizations of Ignatyuk and Reisdorf.

Up to now we have used the average particle multiplicities to compare the statistical-model results with experimental values. In Fig. 11 we add to this comparison the information of the slope parameter of the particle energy

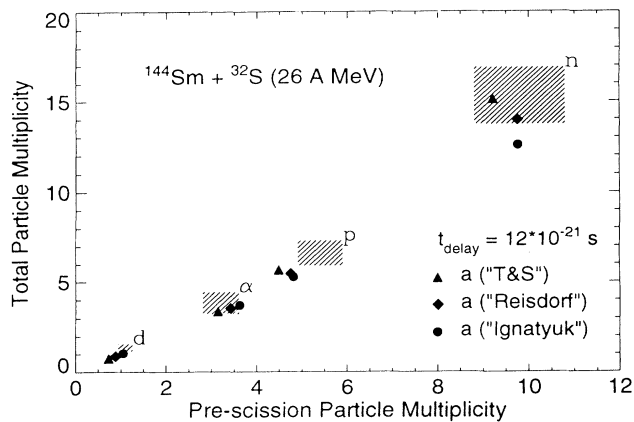


FIG. 10. The correlation of total and pre-scission particle multiplicity for neutron, proton, deuteron, and alpha evaporation. The experimental results are represented by dashed areas and the results of evaporation calculations using different level-density parameters are displayed by filled symbols.

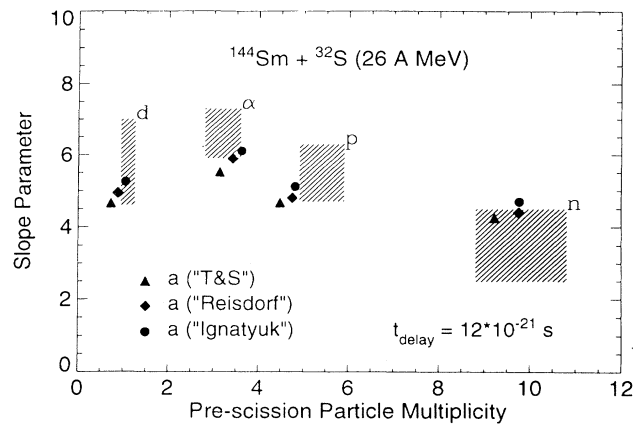


FIG. 11. Same as Fig. 10, but for the correlation of the slope parameter of the energy spectra and the pre-scission particle multiplicity.

spectra. This parameter has been extracted from the measured and computed energy spectra by fits using a Watt spectral shape [$n = \frac{1}{2}$ in Eq. (3)]. The experimental values including the uncertainties are shown by dashed areas, and the values extracted from the computed spectra are displayed by filled symbols. As expected from column 5 of Table II, the Ignatyuk parametrization results in the highest slope parameter, the TS parametrization yields the lowest one. Again, the charged particle energy spectra favor the low level density of Ignatyuk, and the neutron spectra are better described by TS.

In Fig. 12 the energy spectra measured for p , d , and α at $\theta_{\text{lab}} = 148^\circ$ are compared with evaporation computations for the fissioning nucleus, employing the Ignatyuk level-density parametrization and adjusting the computed yield at the proton spectrum. The composite system component being dominant at backward angles, is well described with respect to barrier heights, slope param-

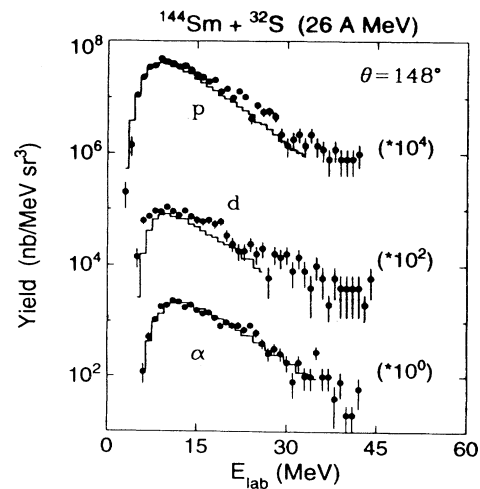


FIG. 12. Comparison of measured and computed particle energy spectra at $\theta_{\text{lab}} = 148^\circ$. The computed spectra have been normalized to the experimental alpha yield.

ters, and relative yield. This agreement adds significant confidence to the statistical model results at excitation energies of 3 MeV/nucleon.

V. SUMMARY

In addition to previously investigated neutron spectra light charged particle spectra have been measured in coincidence with fission fragments for the system $^{144}\text{Sm} + ^{32}\text{S}$ at a bombarding energy of 838 MeV. The energy spectra of protons, deuterons, and alpha particles taken at an angular range which span 67% of 4π were analyzed employing a five source fit procedure to extract values for multiplicity, barrier height, and apparent temperature of the pre-equilibrium as well as the pre- and postscission components of particle emission. Application of the massive transfer model using the extracted multiplicities of the pre-equilibrium component results in a fraction of 71% in linear momentum which is transferred to the composite system. Considering the experimental time resolution and the rough approximations applied, this fraction is in satisfactory agreement with the value of 77% extracted from kinematics by measuring the velocity vectors of the two fission fragments.

The excitation energies deduced from multiplicity and temperature parameters of the pre-equilibrium particle source were used in a statistical-model analysis. The input of these computations also included the spin distribution given by a classical model for dissipative projectile breakup and level-density parameters which account for volume, surface, and curvature effects of the compound system. Comparing measured and computed parameters of energy spectra of fissioning nuclei, we conclude that the correlations between pre-scission and total multiplici-

ty and slope (temperature parameter of the fissioning nucleus) is a sensitive tool to test level-density parameters. Unfortunately, the uncertainties in the experimental values were not sufficient to get quantitative results. Qualitatively we can state, that the energy spectra of particles (p, d, α) emitted at high temperatures can be better described by level-density parameters that are lower than $a = A/9$, whereas neutrons, which are emitted on average at lower excitation energies, prefer level-density parameters higher than $a = A/9$.

Application of the “neutron clock” for the systems $^{32}\text{S} + ^{144,154}\text{Sm}$, ^{197}Au , and ^{232}Th at bombarding energies of 838 MeV has given fission times in the range of $(5-30) \times 10^{-21}$ s [2,3]. We got a satisfactory reproduction of pre-scission particle multiplicities using a fission delay time of $t_{\text{delay}} = 12 \times 10^{-21}$ s, and thus conclude that both clocks, the “neutron clock” and the “charged particle clock,” are equivalent, which is expected as long as the statistical model is applicable.

In the alpha spectra a low-energy component is observed, which is strongly focused in directions perpendicular to the fission axis. Similar observations have been made by other groups, which identified this low-energy component with particles that are emitted close to the scission configuration of the fissioning system. A more detailed analysis of these particles might enable the examination of the shape of the nucleus at scission.

ACKNOWLEDGMENTS

The authors wish to acknowledge the valuable support of the SARA operators in providing us with reliable beams, and obliged to K. Möhring for his model calculations of dissipative projectile breakup.

-
- [1] D. Hilscher and H. Rossner, *Ann. Phys. Fr.* **17**, 471 (1992).
 - [2] D. J. Hinde, D. Hilscher, H. Rossner, B. Gebauer, M. Lehmann, and M. Wilpert, *Phys. Rev. C* **45**, 1229 (1992).
 - [3] E. Mordhorst, M. Strecker, H. Froeben, M. Gasthuber, W. Scobel, B. Gebauer, D. Hilscher, M. Lehmann, H. Rossner, and Th. Wilpert, *Phys. Rev. C* **43**, 716 (1991).
 - [4] H. A. Weidenmüller, *Phys. Lett.* **10**, 331 (1964).
 - [5] M. G. Mustafa, M. Blann, A. V. Ignatyuk, and S. M. Grimes, *Phys. Rev. C* **45**, 1078 (1992).
 - [6] R. Wada, D. Fabris, K. Hagel, G. Nebbia, Y. Lou, M. Gonin, J. B. Natowitz, R. Billerey, B. Cheynis, A. Demeyer, D. Drain, D. Guinet, C. Pastor, J. Alarja, A. Giorni, D. Heuer, C. Morand, J. B. Viano, C. Mazur, C. Ngo, S. Leray, R. Lucas, M. Ribrag, and E. Tomasi, *Phys. Rev. C* **39**, 497 (1989).
 - [7] J. B. Natowitz, M. Gonin, K. Hagel, R. Wada, S. Shlomo, X. Bin, M. Gui, Y. Lou, D. Utley, T. Botting, R. K. Choudhury, L. Cooke, B. Hurst, D. O’Kelly, R. P. Schmitt, W. Turmel, H. Utsunomiya, G. Nebbia, D. Fabris, J. A. Ruiz, G. Nardelli, M. Poggi, R. Zanon, G. Viesti, R. H. Burch, F. Gramegna, G. Prete, D. Drain, B. Chambon, B. Cheynis, D. Guinet, X. C. Hu, A. Demeyer, C. Pastor, A. Giorni, A. Lleres, P. Stassi, J. B. Viano, A. Menchaca Rocha, M. E. Brandan, and P. Gonthier, *Nucl. Phys. A* **538**, 263c (1992).
 - [8] D. Hilscher, H. Rossner, B. Cramer, B. Gebauer, U. Jahnke, M. Lehmann, E. Schwinn, M. Wilpert, Th. Wilpert, H. Froeben, E. Mordhorst, and W. Schobel, *Phys. Rev. Lett.* **62**, 1099 (1989).
 - [9] D. Drain, A. Giorni, D. Hilscher, C. Ristori, J. Alarja, G. Barbier, R. Bertholet, R. Billerey, B. Chambon, B. Cheynis, J. Crançon, A. Dauchy, P. Désesquelles, A. Fontenille, L. Guyon, D. Heuer, A. Lleres, M. Maurel, E. Monnard, C. Morand, H. Nifenecker, C. Pastor, J. Pouxe, H. Rossner, J. Saint-Martin, F. Schussler, P. Stassi, M. Tournier, and J. B. Viano, *Nucl. Instrum. Methods Phys. Res. A* **281**, 528 (1989).
 - [10] F. Benrachi, B. Chambon, B. Cheynis, D. Drain, C. Pastor, D. Seghier, K. Zaid, A. Giorni, D. Heuer, A. Lleres, C. Morand, P. Stassi, and J. B. Viano, *Nucl. Instrum. Methods A* **281**, 137 (1989).
 - [11] F. Benrachi, Ph.D. thesis, Université Claude Bernard, Lyon, 1992.
 - [12] J. Mistretta, Ph.D. thesis, Université Joseph Fourier, Grenoble, 1988.
 - [13] J. P. Lestone, Ph.D. thesis, Australian National University, Canberra, 1990.
 - [14] K. Möhring, T. Srokowski, and D. H. E. Gross, *Nucl. Phys. A* **533**, 333 (1991).
 - [15] H. Rossner, D. Hilscher, D. J. Hinde, B. Gebauer, M. Lehmann, M. Wilpert, and E. Mordhorst, *Phys. Rev. C*

- 40, 2629 (1989).
- [16] Z. Fraenkel, *Phys. Rev.* **156**, 1283 (1967).
- [17] D. E. Fields, K. Kwiatkowski, K. B. Morley, E. Renshaw, J. L. Wile, S. J. Yennello, V. E. Viola, and R. G. Korteling, *Phys. Rev. Lett.* **69**, 3713 (1992).
- [18] E. M. Rastopchin, Yu. B. Ostapenko, M. I. Svirin, and G. N. Smirenkin, *Yad. Fiz.* **49**, 24 (1989) [*Sov. J. Nucl. Phys.* **49**, 15 (1989)].
- [19] W. D. Myers and W. J. Swiatecki, *Ann. Phys.* **84**, 186 (1974).
- [20] J. M. Alexander, M. T. Magda, and S. Landowne, *Phys. Rev. C* **42**, 1092 (1990).
- [21] D. Wilmore and P. E. Hodgson, *Nucl. Phys.* **55**, 673 (1964).
- [22] F. G. Perey, *Phys. Rev.* **131**, 745 (1963).
- [23] J. M. Lohr and W. Haerberli, *Nucl. Phys.* **A232**, 381 (1974).
- [24] J. R. Huizenga and G. Igo, *Nucl. Phys.* **29**, 462 (1962).
- [25] L. C. Vaz and J. M. Alexander, *Z. Phys. A* **318**, 231 (1984).
- [26] A. V. Ignatyuk, M. G. Itkis, and V. N. Okolovich, *Yad. Fiz.* **21**, 1185 (1975) [*Sov. J. Nucl. Phys.* **21**, 612 (1975)].
- [27] W. Reisdorf, *Z. Phys. A* **300**, 227 (1981).
- [28] J. Töke and W. J. Swiatecki, *Nucl. Phys.* **A372**, 141 (1981).